Chapter 9

A Numerical Analysis of Vortex Dislocation in Wake-type Flow with Different Spanwise Nonuniformity

Guocan Ling [1]
The State Key Laboratory of Nonlinear Mechanics, Institute of Mechanics,
Chinese Academy of Sciences, Beijing, 100080, China

Dedicated to Professor Lu Ting on his eightieth birthday

Abstract

Two distinct types of vortex dislocation generated in wake-type flows with different spanwise nonuniformities are numerically studied by DNS. A local spanwise disturbance to the velocity of the coming flow leads to generation of consecutive twisted chain-like vortex dislocations in the middle downstream, which is mainly caused by phase difference between vortex shedding cells, while a stepped variation of velocity in the coming flow yields a periodic vortex splitting-reconnection to form a spot-like dislocation, which is mainly caused by frequency difference between the shedding cells. Dynamics and main features of these dislocations, especially the vortex linkages over the dislocations are clearly described by tracing the substantial modification of vorticity lines and other key flow quantities. Local irregularities in the variations of velocity, vorticity and frequency and transition behavior of the wake flows with vortex dislocations are analyzed.

Keywords: two distinct types of vortex dislocation; wake-type flow; transition behavior; Direct Numerical Simulation

[1] linggc@imech.ac.cn

9.1 Introduction

It has been confirmed that for low Reynolds number the vortex dislocation is a fundamental characteristic of three-dimensionalities of bluff body wakes. Depending on different three-dimensional flow conditions, either in cylinder geometry or in the coming flow, the vortex dislocation may present various fascinating modes or patterns, for instance, vortex "splitting and reconnection", vortex "kinks" or "holes", or a kind of large-scale spot-like vortex dislocations and so forth. Those phenomena can be found in cylinder wakes with diameter variation or nonuniform coming flows, or in the wake of stepped cylinder, as well as in the wake of the cylinder with end effects. Detailed presentations of them can be found in the experimental studies and reviews of Gerrard (1966), Eisenlohr & Eckelmann (1989), Bearman (1992), Lewis & Gharib (1992) , Papangelou (1992), Williamson (1992, 1996), among others. Again, the vortex dislocations may be characterized by "a local break of continuity appearing on the "spinal column" of a main vortex row", which occurs randomly in the natural transition of cylinder wakes (Braza *et al.*, 2001). In those previous works, flow visualization and measurement have provided much information on the generation and evolution of vortex dislocation. Some preliminary analyses on the mechanism based on the inviscid vortex dynamics have been given too. Recently there are few numerical studies on the forced vortex dislocations in wake-type flow (Ling & Xiong, 2001, Ling & Zhao, 2003), and the natural vortex dislocations in the wake transition (Braza *et al.*, 2001). The generation and the influence of the dislocation on the flow transition were reported. The occurrence of vortex dislocations is closely related to the break-up to turbulence and is considered a new mechanism of the wake transition. Moreover, it is associated with the variation of forces acting on the cylinders. Besides, the phenomenon of vortex dislocation can also be observed in three-dimensional evolution of a mixing layer (Dallard & Broward, 1993) and some of other nonlinear waves. Therefore, study of the vortex dislocation has received a great deal of attention.

However, due to its very complex three-dimensional nature the detailed information on the formation and the features of vortex linkages in dislocations are still not yet known thoroughly. The mechanistic explanation given for the vortex dislocation in previous studies was basically based on an inviscid vortex dynamics, which is not capable of offering a complete understanding for the real viscous flows. The physical understanding and the description are far from complete. Moreover, concerning the influence

of the nonuniformity in the coming flow on the vortex dislocation we now only have a little knowledge. Thus, it is believed that to make further numerical study to address those issues is significant.

The purpose of the present work is to study the character of vortex dislocations generated in wake-type flows with different spanwise nonuniformity in coming flow by direct numerical simulation approach. Based on the DNS results the dynamical scenario of the formation of vortex dislocation and the basic features of the dislocations are described by analyzing the substantial modification of voriticity line tracks as well as key quantities of the flow field. Vortex linking, vortex splitting and reconnection in the dislocation produced in real viscous flows are illustrated in detail. The influence of the nonuniformity imposed in the coming flow on the dislocation is reported. Transition behavior and the irregularity of the flow are also studied.

9.2 Numerical simulation and method

In the present calculations, two cases of the nonuniform coming flow are considered, which is taken as

$$U(y,z) = 1.0 - a(z)(2.0 - \cosh(b(z)y^2))\exp(-c^2(z)y^2). \tag{9.1}$$

It is a kind of time-averaged streamwise velocity profile in a cylinder wake at the position where the flow is most unstable. The parameters b and c are determined by referring to DNS results of cylinder wake flow given by Karniadakis and Triantafyllou (1992), and the experimental measurements of Nishioka and Sato (1974). Here $a(z)$ is introduced to express the nonuniformity in momentum defect in the coming flow along the span. For case one, a local spanwise nonuniformity is imposed, and $a(z) = 1.1 + 0.4\exp(-z^2)$, $b = 1.1$, c $= 1.2$. The local disturbance *to* coming flow is introduced near the center of the span and exponentially decayed with the increase of the distance. For case two, a stepped variation of the coming flows is considered, and $a(z) = 1.1, b = 0.9$, c $= 0.9818$ for $|z| < 2.5$ and $a(z) = 1.1, b = 1.1$, c $= 1.2$ for $2.5 \leq |z| \leq 15$, respectively. It is believed that these wake-type flows are unstable. Development of the instability will lead to different vortex street flows, and evolves vortex dislocations, which may have some similar behavior, to some extent, to those in real cylinder wakes with diameter variation.

In the present DNS, compact finite difference-Fourier spectral hybrid

method is used for solving three-dimensional Navier-Stokes equations. A detailed presentation of these equations and the numerical method can be found in Xiong and Ling (1996), Ling & Xiong (2001). The procedure of the method is summarized as follows. In the spanwise direction of the flow, the periodic boundary conditions are assumed. And then we expand all the flow variables into a truncated Fourier series as

$$\varphi(x,y,z,t) = \sum_{m=-N/2}^{N/2-1} \varphi_m(x,y,t)e^{-im\beta z}, \tag{9.2}$$

where x, y and z are the streamwise, vertical, and spanwise directions, respectively. N is the cutoff, and β is the spanwise wavenumber. The three-dimensional incompressible Navier-Stokes equations are written, in primitive variable formation, as

$$\frac{\partial \vec{V}}{\partial t} + (\vec{V}\cdot\nabla)\vec{V} = -\nabla p + \frac{1}{Re}\nabla^2\vec{V}, \tag{9.3}$$

where $\vec{V} = \{u, v, w\}$ are the velocity components in x, y, z directions, respectively, and p is the pressure. The characteristic length D and the velocity scales U_0 are introduced, where U_0 is specified to be the streamwise wake-type inflow velocity $U(y,z)$ at y $= \pm\infty$, and D is chosen such that in non-dimensional variables, $U(D/2,\infty) = \frac{1}{2}[U(0,\infty) + U(\infty,\infty)]$. The Reynolds number is defined as $Re = U_0 D/\nu$, where ν is the kinematic viscosity. Substituting (9.2) into (9.3), we find a system of equations for the rn-th harmonic in a two-dimensional (x,y) domain as

$$\frac{\partial \vec{V}_m}{\partial t} + F_m\left[\left(\vec{V}\cdot\nabla\right)\vec{V}\right] = -\nabla_m p_m + \frac{1}{Re}\nabla_m^2\vec{V}_m, \tag{9.4}$$

where $\nabla_m = \{\partial/\partial x, \partial/\partial y, -im\beta\}$, $\nabla_m^2 = \partial^2/\partial x^2 + \partial^2/\partial y^2 - m^2\beta^2$, and $F_m\left[\left(\vec{V}\cdot\nabla\right)\vec{V}\right]$ is the Fourier transformation of the nonlinear terms. For the time discretization of the equation a third-order mixed explicit-implicit scheme is used. The solution procedure at every time step is split into the following three substeps:

$$\begin{aligned}
\frac{\vec{u}'_m - \sum_{q=0}^{J_i-1}\alpha_q \vec{u}_m^{n-q}}{\Delta t} &= -\sum_{q=0}^{J_e-1}\beta_q F_m\left[(\vec{u}^{n-q}\cdot\nabla)\,\vec{u}^{n-q}\right],\\
\frac{\vec{u}''_m - \vec{u}'_m}{\Delta t} &= -\nabla_m p_m^{n+1},\\
\frac{\gamma_0\vec{u}_m^{n+1} - \vec{u}''_m}{\Delta t} &= \frac{1}{Re}\nabla_m^2\vec{u}_m^{n+1},
\end{aligned} \tag{9.5}$$

where $\vec{u}'_m$, $\vec{u}''_m$ are intermediate velocities; J_i, J_e are parameters for the order of the scheme, and α_q, β_q, γ_0 are appropriately chosen weights. For the third order case, the values of these coefficients, following the study of Karniadakis et al. (1994), are cited as follows:

$$J_e = 3, J_i = 3, \alpha_0 = 3, \alpha_1 = -\frac{3}{2}, \alpha_2 = \frac{1}{3}, \beta_0 = 3, \beta_1 = -3, \beta_2 = 1, \gamma_0 = \frac{11}{6}.$$

To evaluate the nonlinear terms in the split equations, the pseudo-spectral method is adopted, and the fifth order upwind compact scheme is used to approximate the terms. The derivatives of the Fourier coefficients u_m are calculated by the sixth-order center compact schemes. For solving Helmholtz equations for pressure and velocity, a nine-point compact scheme of fourth-order central compact scheme is derived and used for nonhomogeneous term calculations, which is

$$\frac{10(\varphi_1 + \varphi_3) - 2(\varphi_2 + \varphi_4) + (\varphi_5 + \varphi_6 + \varphi_7 + \varphi_8) - 20\varphi_0}{(\Delta x)^2}$$

$$+ \frac{10(\varphi_2 + \varphi_4) - 2(\varphi_1 + \varphi_3) + (\varphi_5 + \varphi_6 + \varphi_7 + \varphi_8) - 20\varphi_0}{(\Delta y)^2}$$

$$(8\varphi_0 + \varphi_1 + \varphi_2 + \varphi_3 + \varphi_4)b = (8f_0 + f_1 + f_2 + f_3 + f_4).$$

For the pressure boundary conditions, with formulas (9.4) and (9.5), the semi-discretized representation can be written as

$$\begin{aligned} \frac{\partial p_m^{n+1}}{\partial n} &= \vec{n} \cdot \left\{ -\frac{\partial \vec{u}_m}{\partial t} + \frac{1}{Re}\nabla^2 \vec{u}_m^{n+1} - \sum_{q=0}^{J_e-1} \beta_q F_m \left[(\vec{u}^{n-q} \cdot \nabla)\vec{u}^{n-q}\right] \right\} \\ &= \vec{n} \cdot \left\{ -\frac{\partial \vec{u}_m}{\partial t} - \frac{1}{Re} F_m \left[\nabla \times \vec{\Omega}^n\right] - \sum_{q=0}^{J_e-1} \beta_q F_m \left[(\vec{u}^{n-q} \cdot \nabla)\vec{u}^{n-q}\right] \right\} \end{aligned} \tag{9.6}$$

where $\nabla^2 \vec{u} = \mathrm{UD} - \nabla \times \vec{\Omega}$, $\vec{\Omega} \equiv \mathrm{V} \times \vec{u}$, $D = \nabla \cdot \vec{u}$. By forcing $D^{n+1} \equiv 0$ in each time step and replacing $\nabla \times \vec{\Omega}^{n+1}$ by $\nabla \times \vec{\Omega}^n$, the divergence-free constraint can be well satisfied on the boundaries.

For a finite computing domain, the non-reflecting boundary condition for outflow in physical space is suggested:

$$\frac{\partial \vec{u}}{dt} + u\frac{\partial \vec{u}}{dx} = \frac{1}{Re}\left(\frac{\partial^2 \vec{u}}{\partial y^2}\right). \tag{9.7}$$

The corresponding spectral form used in the computation is

$$\frac{\partial \vec{u}_m}{\partial t} + F_m \left[u \frac{\partial \vec{u}}{\partial x} \right] = \frac{1}{Re} \left(\frac{\partial^2 \vec{u}_m}{\partial y^2} - m^2 \beta^2 \vec{u}_m \right) \tag{9.8}$$

Equation (9.8) must be solved simultaneously with the same third-order mixed explicit-implicit schemes adopted for Navier-Stokes equations in the inner domain.

In the present computation, Reynolds number is taken as 200. The computational domains are 100, **30,** 30 in streamwise, vertical and spanwise directions, respectively. The cutoff of the truncated Fourier series is $N = 64$ and the corresponding grid points in $x - y$ plane is 202 x **62.** The numerical code used in the present work has been verified first. It shows that evolution of the wake-type flow without the local spanwise non-uniformity results in a normal Kármán vortex street with a Strouhal number of 0.189, which is well compared with both numerical simulation of wake-type flow evolution ($St = 0.195$, see Karniadakis and Triantafyllou, 1992) and DNS results of flow around cylinder ($St = 0.179$, see Triantafyllou and Karniadakis, 1990).

9.3 Numerical results

The present DNS results have shown that spatial temporal evolution of the coming flows leads to two different types of vortex street flow with two distinct types of vortex dislocation generated in the middle downstream of the flows, respectively. Variation of the vorticity line tracks, isosurface of vorticity, vorticity component contours and fluctuating velocity distributions are used to describe the whole picture of the dislocation and its development in space.

9.3.1 *Local spanwise nonuniformity*

For this case, a series of symmetric twisted chain-like vortex dis locations is generated in the middle downstream as shown by the isosurface of vorticity in Fig. 9.1. The vortex dislocation occurs consecutively based on the background shedding flow, and is characterized by an undulated spanwise vortex connected by streamwise and vertical vortex branches. Behaviors of representative vorticity lines emitting from different positions in main vortex show that, as the flow travels downstream, these lines undergo a substantial modification from spanwise direction to streamwise and vertical ones. In particular, in the upstream region, the spanwise vortex lines

start to undulate in the spanwise direction, then undergo a stronger distortion near the central area (Fig. 9.2). In the middle downstream, a set of vortex lines pass across the span with a big distortion near the central area, and the others bend into upstream, then after turning 180 degree go into the adjacent main vortex. It is interesting to note that some vortex lines starting from the different vertical positions of the same vortex will go back to downstream and join the next spanwise vortex (Fig. **9.3).** That is the phenomenon of vortex splitting and reconnection occurred in the vortex dislocation. Calculation shows that the real behavior of the phenomenon is some vorticity lines, located at the outer region of a vortex roll (vorticity blob), changing their directions, under the interaction with adjacent vortices, from original spanwise direction to streamwise, vertical direction and further joining to their neighboring main vortices with opposite sign. In present calculation, the initial phase and strength of shedding vortices are evaluated. Due to the local spanwise nonuniformity of the incoming flow, there are pronounced differences in phase and strength between shedding cells. The results demonstrated that these differences make spanwise vorticity lines curve to produce vorticity component in other two directions. Moreover the vortex splitting and reconnection are only produced at some positions where the rate of phase difference reaches a maximum value; meantime three-dimensional vortex dislocation structures are formed. It is in agreement with the experimental study of Eisenlohr & Eckelman (1989).

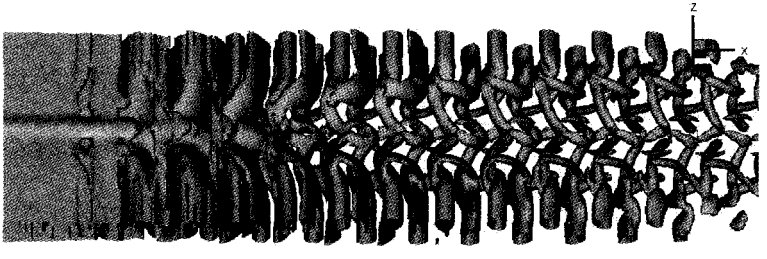

Fig. 9.1 Symmetric twisted chain-like vortex dislocation pattern, visualized by Isosurface of vorticity $|\omega| = 0.12$, at $t = 260$.

In summary, for the present case, the basic features of vortex linking in vortex dislocation, as shown in Figs. 9.2, **9.3** and 9.4, can be briefly described in the following outline: (1) large undulated spanwise vortex roll;

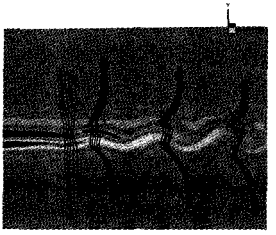

Fig. 9.2 Spatial variation of vorticity line tracks

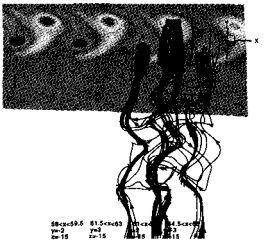

Fig. **9.3** The vortex linkages in vortex dislocation. Vortex splitting and reconnection with adjacent primary spanwise vortices are shown by variation of vorticity line tracks.

Fig. 9.4 End view of vortex linkages in vortex dislocation. Vorticity lines wind round the neighboring vortices.

(2) some split spanwise vortex lines diverting their direction and connecting with adjacent vortices by a cross-vortex street mode; **(3)** the distorted vortex lines wind round their neighboring spanwise vortices. These features coincide with those shown in Fig. 9.1. The vortex dislocation is mainly caused by the phase difference between shedding vortices.

The influence of vortex dislocation on the flow transition is examined by irregular variation of some key quantities of flow field. Time series of fluctuation velocity components, at the positions near the center part of the span present a pronounced irregularity and accompanied by a low frequency modulation, while near both sides of the span the variation of velocity is quasi-periodic, similar to that induced by a common Kármán vortex street.

In spectra of velocity components several peak values are found at a basic frequency, its harmonics and at a low frequency. The basic one corresponds the vortex shedding of the base flow. Near the vortex dislocation the spectra show the variation of frequency is irregular. In addition to those, the vorticity line tracks in vortex dislocation, as shown in Fig. 9.4, also present a chaotic behavior. It is clear that the appearance of the vortex dislocation and its breakdown make flow irregular, which is closely related to the break up to the local turbulence and the spatial chaos of the flow.

9.3.2 *Stepped spanwise nonuniformity*

For this case, the vortex dislocation occurs periodically near the steps of the incoming flow velocity in the span and caused mainly by the frequency difference between shedding cells over the steps.The main features are visualized by isosurfaces of vorticity and vorticity component in stream direction, as shown in Figs. 9.5 and 9.6. The vortex dislocation is characterized by undulated spanwise vortex roll and vortex splitting from it. The split spanwise vorticity lines turn their direction towards upstream becoming streamwise vortex branch and then turn further joining a neighboring main vortex. Several vortex patterns of this kind constitute a periodic spot-like vortex dislocation and travel downstream periodically.

(a)$t = 316$ (b)$t = 334$

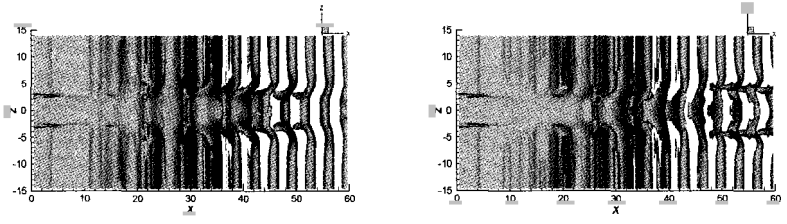

Fig. 9.5 Visualization of spot-like dislocation pattern, which consists of several vortex splitting and reconnections shown by the isosurface of vorticity $|\omega| = 0.15$.

(a)$t = 316$ (b)$t = 334$

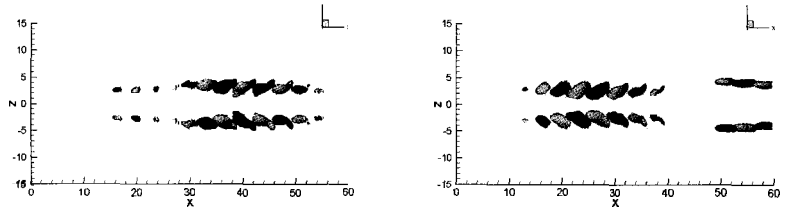

Fig. 9.6 Iso-surface of streamwise vorticity in vortex dislocation $\omega_x = 0.11$ (gray) and $\omega_x = -0\ 11$ (black).

Time series of fluctuation velocity components and their spectra are examined. A sample of these behaviors is shown in Figs. 9.7, 9.8 and 9.9, respectively. In the center region of the span, (i.e. for $|z| \leq 3$), a pronounced velocity modulation occurs periodically over the time series, which corresponds to the appearance of the vortex dislocation, while away

from the center region, the velocity presents a regular variation like that produced by a common Kármán vortex street. In the spectra of vertical velocity component (Fig. 9.8), there are two pronounced peaks at $f_1 = 0.117$ (for $z = 0$ to 4) and $f_2 = 0.141$ (for $z \geq 4$). They are incommensurable, and correspond to the vortex shedding in the center region and outer region, respectively. A peak at the difference of these two frequencies is found in low frequency area. It is the 'beat' between the two sets of vortex shedding and is just the period of the spot-like vortex dislocation. It is the result of nonlinear interaction between these two frequencies. However in spectra for spanwise velocity component as shown in Fig. 9.9 multi-peak values at different frequencies are presented. The evolution with time of the velocity is irregular. The characteristic of time-frequency of velocity components at different positions in flow field is further studied by using wavelet analysis. A sample of these results is given by Fig. 9.10. It shows that at a point in the flow field the dominant frequency varies with time and shifts between two main frequencies. This variation is due to the generation of vortex dislocation and its passage through the position.

Based on the DNS results the Proper Orthogonal Decomposition (POD) analysis of wake-type flow with vortex dislocation has been performed too. The nonlinearity and the transition behavior of the flow are further analyzed. For details, reader is referred to the work of Zhao & Ling (2003).

9.4 Concluding remarks

The present study has shown that two kinds of vortex dislocation, the symmetric twisted chain-like vortex dislocation and the spot-like dislocation, are generated in wake-type flows. The characteristic and dynamics of the vortex dislocations are dependent on the coming flow nonuniformity in spanwise direction. The two kinds of dislocation are mainly caused by the differences in phase and in frequency, respectively. The formation and the structure of the vortex dislocations, as well as the real linkages over the dislocations, have been clearly described by substantial modification of vorticity field, especially, by the vortex line behavior, and the other flow field quantities. Large distortion and splitting of the original spanwise vortex roll, and the reconnection in viscous vortex dislocation are shown in detail. Frequency variation in wake flow is examined. The local irregularities in variation of velocity, vorticity and frequency, characterizing the transition behavior of the two wake flows with vortex dislocations, are reported.

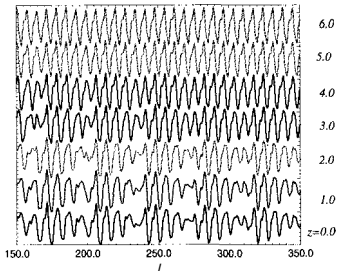

Fig. 9.7 Time series of vertical velocity component along the span at $(x, y) = (30, 0.5)$.

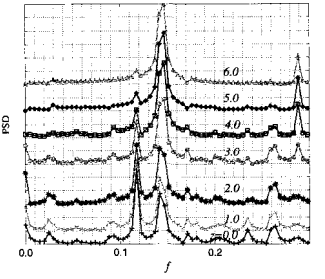

Fig. 9.8 Spectra of vertical velocity component along the span at $(x, y) = (30, 0.5)$.

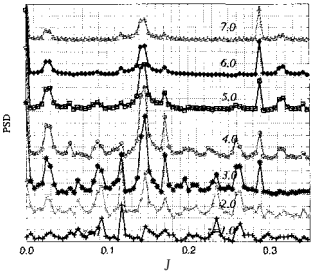

Fig. 9.9 Spectra of spanwise velocity component along the span at $(x, y) = (30, 0.5)$.

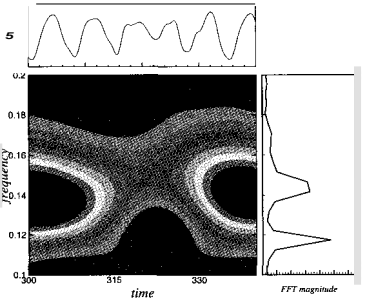

Fig. 9.10 Wavelet analysis of vertical velocity component at $(x, y, z) = (45, 0.5, 0)$.

Acknowledgment

This work is supported by the National Natural Science Foundation of China under Grant No.10272104, and partially by CAS Innovation projects "study on Complex Flows". The calculation in present work is finished by Dr. Hongliang Zhao. His contribution is also acknowledged.

Bibliography

Bearman, P.W. 1992 Challenging problems in bluff body wakes. *Bluff-Body Wakes, Dynamics and Instabilities, IUTAM Symposium.* Gottingen: Springer-Verlag.

Braza, M., Faghani, D. & Persillson, H. 2001 Successive stages and the role of

natural vortex dislocation in three-dimensional wake transition. *J. Fluid Mech.* **439**:1-41.

Dallard, T. & Browand, F.K. 1993 The growth of large scales at defect sites in the plane mixing layer. *J. Fluid Mech.* **247**:339-368.

Eisenlohr, H. & Eckelemann, H. 1989 Vortex splitting and its consequences in vortex street wake of cylinders at low Reynolds number. *Phys. Fluids A* **1**:189-192.

Gerrard J.H. 1966 The three-dimensional structure of the wake of a circular cylinder. *J. Fluid Mech.* **25**:143-164.

Karniadakis, G.E. & Triantafyllou, G.S. 1992 Three-dimensional dynamics and transition to turbulence in the wake of bluff objects. *J. Fluid Mech.* **238**:1-30.

Kaniadakis, G.E., Israeli, S.A. & Orzag, S.A. 1994 High-order splitting methods for the incompressible Navier-Stokes equations. J. Comput. Phys. **97**:414.

Lewis, C.G. & Gharib, M. 1992 An exploration of wake three-dimensionalities caused by a local discontinuity in cylinder diameter. *Phys. Fluids A* **4**:104-117.

Ling, G.C. & Xiong, Z.M. 2001 Generation of large-scale vortex dislocations in a three-dimensional wake-type flow. *Science in China (series A)* **4**(12):1585-1595.

Ling, G.C. & Zhao H.L. 2003 Structure of vortex dislocation in a wake-type flow. CHIN. PHYS. LETT. **20**(3):383-385.

Nishioka, M. & Sato, H. 1974 Measurements of velocity distributions in the wake of a circular cylinder at low Reynolds numbers. *J. Fluid Mech.* **65**:97-112.

Papangelou, A. 1992 Vortex shedding from slender cones at low Reynolds numbers. *Bluff-Body Wakes, Dynamics and Instabilities, IUTAM Symposium.* Gottingen: Springer-Verlag.

Triantafyllou, G.S., Karniadakis, G.E. 1990 Computational reducibility of unsteady viscous flow. *Phys. Fluids A* **2**:653-658.

Willamson, C.H.K. 1992 The natural and forced formation of spot-like vortex dislocations in the transition of a wake. *J. Fluid Mech.* **243**:393-441.

Willamson, C.H.K. 1996 Vortex dynamics in the cylinder wake. *Annu. Rev. Mech.* **28**:477-539.

Xiong, Z.M. & Ling, G.C. 1996 Compact finite difference-Fourier spectral method for three-dimensional incompressible Navier-Stokes equations. *ACTA. Mechanica Sinica* **12**(4):296-306.

Zhao, H.L. & Ling, G.C. 2003 Low-dimensional dynamical systems for a wake-type shear flow with vortex dislocations. *Fluid Dynamics Research* **33**:299-312.